Physics Letters B 718 (2013) 1186–1193

Contents lists available at SciVerse ScienceDirect

Physics Letters B

www.elsevier.com/locate/physletb

Determination of neutrino mass hierarchy by 21 cm line and CMB B-mode polarization observations

Yoshihiko Oyama [a,*], Akie Shimizu [a], Kazunori Kohri [a,b]

[a] The Graduate University for Advanced Studies (SOKENDAI), 1-1 Oho, Tsukuba 305-0801, Japan
[b] Institute of Particle and Nuclear Studies, KEK, 1-1 Oho, Tsukuba 305-0801, Japan

ARTICLE INFO

Article history:
Received 21 July 2012
Received in revised form 9 November 2012
Accepted 21 December 2012
Available online 28 December 2012
Editor: T. Yanagida

ABSTRACT

We focus on the ongoing and future observations for both the 21 cm line and the CMB B-mode polarization produced by a CMB lensing, and study their sensitivities to the effective number of neutrino species, the total neutrino mass, and the neutrino mass hierarchy. We find that combining the CMB observations with future square kilometer arrays optimized for 21 cm line such as Omniscope can determine the neutrino mass hierarchy at 2σ. We also show that a more feasible combination of Planck + PolarBear and SKA can strongly improve errors of the bounds on the total neutrino mass and the effective number of neutrino species to be $\Delta\Sigma m_\nu \sim 0.12$ eV and $\Delta N_\nu \sim 0.38$ at 2σ, respectively.

1. Introduction

Since the discoveries of neutrino masses by Super-Kamiokande through neutrino oscillation experiments in 1998, the standard model of particle physics has been forced to change to theoretically include the neutrino masses.

So far only mass-squared differences of the neutrinos have been measured by neutrino oscillation experiments, which are reported to be $\Delta m^2_{21} \equiv m^2_2 - m^2_1 = 7.59^{+0.19}_{-0.21} \times 10^{-5}$ eV^2 [1] and $\Delta m^2_{32} \equiv m^2_3 - m^2_2 = 2.43^{+0.13}_{-0.13} \times 10^{-3}$ eV^2 [2]. However, absolute values and their hierarchical structure (normal or inverted) have not been obtained yet although information for them is indispensable to build such new particle physics models.

In particle physics, some new ideas and new future experiments based on those ideas have been proposed to observe the absolute values and/or the hierarchy of neutrino masses, e.g., through tritium beta decay in KATRIN experiment [3], neutrinoless double-beta decay [4], atmospheric neutrinos in the proposed iron calorimeter at INO [5,6] and the upgrade of the IceCube detector (PINGU) [7], and long-baseline oscillation experiments, e.g., NOνA [8], J-PARC to Korea (T2KK) [9,10] and Oki island (T2KO) [11], and CERN to Super-Kamiokande with high energy (5 GeV) neutrino beam [12].

On the other hand, such nonzero neutrino masses affect cosmology significantly because relativistic neutrinos prohibit the perturbation from evolving, due to following two reasons. First of all, in general relativity, the density perturbation of a relativistic particle can hardly evolve at all before it becomes nonrelativistic. Second a relativistic neutrino erases its own density perturbation up to a horizon scale through its free streaming at every cosmic time. By measuring spectra of density perturbations by using observations of cosmic microwave background (CMB) anisotropies and large-scale structure (LSS), we could constrain the total neutrino mass Σm_ν [13–29] and the effective number of neutrino species N_ν [22,23,25–31]. So far the robust upper bound on Σm_ν has been obtained to be $\Sigma m_\nu < 0.62$ eV (95% C.L.) (see Ref. [26] and references therein) by these cosmological observations. For forecasts by future CMB observations, see also Refs. [32,33].

In addition, by observing power spectrum of cosmological 21 cm radiation fluctuation, we will be able to obtain independent useful information for the neutrino masses [34–37]. That is because the 21 cm radiation is emitted (1) long after the CMB epoch (at a redshift $z \ll 10^3$) and (2) before an onset of the LSS formation. The former condition (1) gives us information on smaller neutrino mass ($\lesssim 0.1$ eV). The latter condition (2) means we can treat only a linear regime of the matter perturbation, which can be analytically calculated unlike the LSS case.

In actual analyses, it should be essential that we combine data of the 21 cm with that of the CMB observations because they complementary constrain cosmological parameter spaces each other. Leaving aside minded neutrino parameters, for example, the former is quite sensitive to the dark energy density, but the latter is relatively insensitive to it. On the other hand, the former has only a mild sensitivity to the normalization of the matter perturbation, but the latter has an obvious sensitivity to it by definition. In pioneering works by [36], the authors tried to constrain the

* Corresponding author.
E-mail address: oyamayo@post.kek.jp (Y. Oyama).

0370-2693
http://dx.doi.org/10.1016/j.physletb.2012.12.053

neutrino mass hierarchy by combining Planck satellite with future 21 cm observations in case of relatively degenerate neutrino masses $\Sigma m_\nu \sim 0.3$ eV.

Here, however, we additionally include analyses of the CMB B-mode polarization produced by a CMB lensing. This gives us more detailed information on the matter power spectrum at later epochs, which means it has better sensitivities for smaller neutrino masses down to $\lesssim 0.1$ eV. That is essential to distinguish the normal hierarchy from the inverted one. In particular we adopt ongoing and future CMB observations such as POLARBEAR and CMBPol, which have much better sensitivities to the B-mode. For ongoing and future 21 cm observations, we adopt MWA, SKA and Omniscope experiments. We forecast possible allowed parameter regions for both neutrino masses and effective number of neutrino species when we use the above-mentioned ongoing and future observations of the 21 cm and the CMB. In particular we propose a nice combination of neutrino masses, $r_\nu = (m_3 - m_1)/\Sigma m_\nu$ to make the mass hierarchy bring to light as is explained in the text.

2. 21 cm radiation

Here we briefly review basic methods to use the 21 cm line observations as a cosmological probe. For further details, we refer readers to Refs. [34,38].

2.1. Power spectrum of 21 cm radiation

The 21 cm line of the neutral hydrogen atom is emitted by hyperfine splitting of the 1S ground state due to an interaction of magnetic moments of proton and electron. Spin temperature T_S of neutral hydrogen gas is defined through a ratio between number densities of hydrogen atom in the 1S triplet and 1S singlet levels, $n_1/n_0 \equiv (g_1/g_0)\exp(-T_\star/T_S)$. where $T_\star \equiv hc/k_B\lambda_{21} = 0.068$ K with λ_{21} ($\simeq 21$ cm) being the wave length of the 21 cm line at a rest frame, and $g_1/g_0 = 3$ is the ratio of spin degeneracy factors of the two levels. A difference between the observed 21 cm line brightness temperature at redshift z and the CMB temperature $T_{\rm CMB}$ is given by

$$T_b(\mathbf{x}) \approx 27 x_{\rm HI}(1+\delta_b)\left(\frac{\Omega_b h^2}{0.023}\right)\left(\frac{0.15}{\Omega_m h^2}\frac{1+z}{10}\right)^{1/2} \times \left(\frac{T_S - T_{\rm CMB}}{T_S}\right)\left(\frac{H(z)/(1+z)}{dv_\parallel/dr_\parallel}\right) \text{mK}, \quad (1)$$

where $x_{\rm HI}$ is the neutral fraction of hydrogen, δ_b is the hydrogen density fluctuation, and $dv_\parallel/dr_\parallel$ is the gradient of the proper velocity along the line of sight due to both the Hubble expansion and the peculiar velocity.

In general, T_b is sensitive to details of intergalactic medium (IGM). However, with a few reasonable assumptions we can omit this dependence [39–41]. At an epoch of reionization (EOR) long after star formation begins, X-ray background produced by early stellar remnants has heated the IGM. Therefore a gas kinetic temperature T_K could be much higher than the CMB temperature $T_{\rm CMB}$. Furthermore the star formation produces a large background of Lyα photons sufficient to couple T_S to T_K via the Wouthuysen–Field effect [42,43]. In this scenario, we are justified in taking $T_{\rm CMB} \ll T_K \sim T_S$ at $z \lesssim 10$, so that T_b does not depend on T_S.

In addition, we adopt following assumptions for the EOR in the same manner as [36,44]. If the IGM is fully neutral, fluctuations of the 21 cm radiation arise only from density fluctuations. In this limit, we can write the power spectrum of the 21 cm line brightness fluctuation $P_{21}(\mathbf{k})$ as [36]

$$P_{21}(\mathbf{k}, z) = \bar{T}_b^2(z)\left(1+\mu^2\right)^2 P_{\delta\delta}(k, z). \quad (2)$$

Here $P_{21}(\mathbf{k}, z)$ is defined by $\langle \delta T_b(\mathbf{k}) \delta T_b^*(\mathbf{k}')\rangle \equiv (2\pi)^3\delta^3(\mathbf{k} - \mathbf{k}')P_{21}(\mathbf{k})$, where $\delta T_b \equiv T_b - \bar{T}_b$ is the deviation from a spatially averaged brightness temperature $\bar{T}_b$, $P_{\delta\delta}$ is the matter power spectrum, and $\mu = \hat{\mathbf{k}}\cdot\hat{\mathbf{n}}$ is the cosine of the angle between the wave number $\mathbf{k}$ and the line of sight. In principle, $\bar{T}_b$ can be calculated although it depends on the unknown ionization and thermal history. Therefore we treat $\bar{T}_b$ as a free parameter to be measured.

The power spectrum $P_{21}(\mathbf{k}, z)$ and the comoving wave number $\mathbf{k}$ are not directly measured by the observations of 21 cm radiation [45,46]. Instead, here we define $\mathbf{u}$ as the Fourier dual of $\boldsymbol{\Theta} \equiv \theta_i\hat{e}_i + \theta_j\hat{e}_j + \Delta f\hat{e}_k$, where θ_i and θ_j determine an angular location on the sky plane and Δf shows the frequency difference from the central redshift of a z bin. The vector $\mathbf{u}$ and its function $P_{21}(\mathbf{u}, z)$ are directly measured by the observations. Relationships between $\mathbf{u} \equiv u_i\hat{e}_i + u_j\hat{e}_j + u_\parallel\hat{e}_k$ and $\mathbf{k}$ are represented by $\mathbf{u}_\perp \equiv u_i\hat{e}_i + u_j\hat{e}_j = d_A(z)\mathbf{k}_\perp = 2\pi\mathbf{L}/\lambda$, and $u_\parallel = y(z)k_\parallel$. Here "$\perp$" denotes the vector component perpendicular to the line of sight. "$\parallel$" denotes the component in the line of sight. $d_A(z)$ is the comoving angular diameter distance to a given redshift. $y(z) = \lambda_{21}(1+z)^2/H(z)$ means the conversion factor between comoving distance intervals and frequency intervals Δf. $\mathbf{L}$ is the baseline vector of an interferometer. $\lambda = \lambda_{21}(1+z)$ denotes the observed wave length of the redshifted 21 cm line. In $\mathbf{u}$ space, the power spectrum $P_{21}(\mathbf{u}, z)$ is defined by $\langle \delta T_b(\mathbf{u}) \delta T_b^*(\mathbf{u}')\rangle \equiv (2\pi)^3\delta^3(\mathbf{u} - \mathbf{u}')P_{21}(\mathbf{u})$. Then, the relation between $P_{21}(\mathbf{u}, z)$ and $P_{21}(\mathbf{k}, z)$ is given by

$$P_{21}(\mathbf{u}, z) = \frac{1}{d_A^2(z)\,y(z)}P_{21}(\mathbf{k}, z). \quad (3)$$

We perform our analyses in terms of $P_{21}(\mathbf{u}, z)$ since this quantity is directly measurable without any cosmological assumptions. For methods of foreground removals, see also recent discussions about independent component analysis (ICA) algorithm, FastICA [47] which will be developed in terms of the ongoing LOFAR observation [48].

2.2. Effects of neutrino masses on power spectrum

The massive neutrinos affect the growth of the matter density perturbation mainly due to following two physical mechanisms. [49]. First of all, a massive neutrino ν_i (even with its light mass $m_{\nu_i} \lesssim 0.3$ eV) becomes nonrelativistic at $T \sim m_{\nu_i}$ and has contributed to the energy density of cold dark matter (CDM), which changes the matter-radiation equality epoch and has changed an expansion rate of the universe since that time. When we fix the total mass of neutrinos Σm_ν ($\lesssim 0.3$ eV), only the latter effect is effective. Second, the matter density perturbations on small scales can be suppressed due to the neutrinos' free-streaming. As long as neutrinos are relativistic, they travel at speed of light, and their free-streaming scales are approximately equal to the Hubble horizon. Then the free-streaming effect erases their own perturbations within such scales.

Compared with the standard ΛCDM models where three massless active neutrinos are assumed, we will consider two more freedoms. First one is an introduction of the effective number of neutrino species N_ν, which counts generations of relativistic neutrinos before the matter-radiation equality epoch and should not be equal to three. Second one is the neutrino mass hierarchy. It is clear that a change of N_ν affects the epoch of matter-radiation equality. On the other hand, the neutrino mass hierarchy affects both the free-streaming scales and the expansion rate as was mentioned above [50]. In terms of the observations of the 21 cm signal, the minimum cutoff of the wave number is given by $k_{\rm min} = 2\pi/(yB) \sim 6\times 10^{-2}h$ Mpc^{-1} (see Section 2.3) while the wave number corresponding to the neutrino free-streaming scale

Table 1
Specifications for each interferometers. $L_{\rm min}$ ($L_{\rm max}$) is the minimum (maximum) baseline. For MWA, we assume a single redshift slice centered at $z=8$. For SKA and Omniscope, the observed redshift range is $z=7.8$–10.3, and we divide the range into five redshift slices with thickness $\Delta z\approx 0.5$. For each experiment, bandwidth is $B=8$ MHz, and we assumed observations for 8000 h on two places in the sky. We assume that the effective collecting area A_e is proportional to λ^2 for MWA and SKA. For Omniscope, both A_e and FOV are fixed.

Experiment	N_{ant}	$A_e(z=8)$ [m^2]	$L_{\rm min}$ [m]	$L_{\rm max}$ [km]	FOV [deg^2]	z
MWA	500	14	4	1.5	$\pi 16^2$	7.8–8.2
SKA	5000	120	10	5	$\pi 5.6^2$	7.8–10.2
Omniscope	10^6	1	1	1	2.1×10^4	7.8–10.2

is $k_{\rm free}\lesssim 10^{-2}h$ Mpc^{-1}. Therefore the main feature of the modification of the matter density fluctuation due to the change of the mass hierarchy comes from the modification of the cosmic expansion when we fix the total matter density at the present time.

2.3. Forecasting methods and interferometers

Here we summarize future observations of the 21 cm signals emitted at the EOR. We also provide a brief review of the Fisher matrix formalism for the 21 cm observations. We consider MWA [51], SKA [52] and Omniscope [53] for future observations. The summary of the detailed specifications is listed in Table 1. Each interferometer has its own different noise power spectrum,

$$P_N(\mathbf{u}_\perp,z)=\left(\frac{\lambda^2(z)T_{\rm sys}(z)}{A_e(z)}\right)^2\frac{1}{t_0 n(u_\perp)}, \tag{4}$$

which affects sensitivities to the 21 cm signals. Here $T_{\rm sys}\simeq 280[(1+z)/7.4]^{2.3}$ K is the system temperature [54], t_0 is the total observation time, and A_e is the effective collecting area of each antenna tile. The effect of the configuration of the antennae is encoded in the number density of baseline $n(u_\perp)$. In order to calculate $n(u_\perp)$, we have to assume a realization of antenna density profiles for each interferometer. For MWA, we take 500 antennae distributed with a filled nucleus of radius 20 m surrounded by the remainder of the antennae distributed with an r^{-2} antenna density profile out to 750 m [55]. For SKA, we distribute 20% of a total of 5000 antennae within a 1 km radius and take the antennae distributed with a nucleus surrounded by an r^{-2} antenna density profile in the same way as those of MWA. These antennae are surrounded by a further 30% of the total antennae in a uniform density annulus of outer radius 6 km [36]. The remainder of the antennae is distributed at larger distances sparsely to be useful for power spectrum measurements. Finally, we consider Omniscope that is a future square-kilometer collecting area array optimized for observations of the 21 cm signal. In case of Omniscope, we take all of antennae distributed with a filled nucleus according to [45].

To forecast 1 σ errors of cosmological parameters, we use the Fisher matrix formalism [56]. For the observations of the 21 cm signal, the Fisher matrix for cosmological parameters p_i is expressed as [57]

$$\mathbf{F}_{ij}^{21\ {\rm cm}}=\sum_{\rm pixels}\frac{1}{[\delta P_{21}(\mathbf{u})]^2}\left(\frac{\partial P_{21}(\mathbf{u})}{\partial p_i}\right)\left(\frac{\partial P_{21}(\mathbf{u})}{\partial p_j}\right), \tag{5}$$

where we sum only over half the Fourier space. The Fisher matrix determines the errors of the parameter p_i to be

$$\Delta p_i\geqslant\sqrt{\left(\mathbf{F}^{-1}\right)_{ii}}. \tag{6}$$

The error of the power spectrum measurement $\delta P_{21}(\mathbf{u})$ in a pixel at $\mathbf{u}$ consists of a sum of the sample variance and the thermal detector noise. It is expressed as

$$\delta P_{21}(\mathbf{u})=\frac{P_{21}(\mathbf{u})+P_N(u_\perp)}{N_c^{1/2}}, \tag{7}$$

where $N_c=2\pi k_\perp\Delta k_\perp\Delta k_\parallel V(z)/(2\pi)^3$ is the number of independent modes in an annulus summing over the azimuthal angle, $V(z)=d_A(z)^2y(z)B\times{\rm FOV}$ is the survey volume, B is the bandwidth, and FOV ($\approx\lambda^2/A_e$) denotes the field of view of the interferometer. For each experiment, we take account of the presence of foregrounds and adopt a cutoff at $2\pi/(yB)\leqslant k_\parallel$ [57]. We also take a maximum value of k to be $k_{\rm max}=3h$ Mpc^{-1} beyond which nonlinear effects become important and exclude all information for $k_{\rm max}<k$.

For each experiment, we assume a specific redshift range as follows [44]. We consider Ly-α forests in absorption spectra of quasars and assume that reionization occurred sharply at $z=7.5$. For an upper limit on the accessible redshift range, we take it to be $z\lesssim 10$ because of increasing foregrounds and uncertainty in the spin temperature at higher redshifts. For the above reasons, we assume that the observed redshift range of EOR is 7.8–10.2. Only for MWA, we assume a single redshift slice centered at $z=8$.

When we calculate the Fisher matrix, we choose the following basic set of cosmological parameters: the energy density of matter $\Omega_m h^2$, baryon $\Omega_b h^2$, dark energy Ω_Λ, the scalar spectral index n_s, the scalar fluctuation amplitude A_s (the pivot scale is taken to be $k_{\rm pivot}=0.002$ Mpc^{-1}), the reionization optical depth τ, Helium fraction $Y_{\rm He}$, and the total neutrino mass $\Sigma m_\nu=m_1+m_2+m_3$. Fiducial values of these parameters (except for Σm_ν) are adopted to be $(\Omega_m h^2,\Omega_b h^2,\Omega_\Lambda,n_s,A_s,\tau,Y_{\rm He})=(0.147,0.023,0.7,0.95,24\times 10^{-10},0.1,0.24)$. We set a range of the fiducial value of Σm_ν to be $\Sigma m_\nu=0.05$–0.3 eV. Besides these parameters, the brightness temperature of 21 cm radiation $\bar{T}_b(z)$ can be taken as a free parameter. In this study, we adopt the fiducial values of $\bar{T}_b(z)$ to be $(\bar{T}_b(8),\bar{T}_b(8.5),\bar{T}_b(9),\bar{T}_b(9.5),\bar{T}_b(10))=(26,26,27,27,28)$ in units of mK.

Additionally, we separately study following two cases:

(A) Effective number of neutrino species.

We add one more parameter of the effective number of neutrino species N_ν to the fiducial set of the parameters. The fiducial value of this parameter is set to be $N_\nu=3.04$. In this analysis, we assumed three species of massive neutrinos + an extra relativistic component.

(B) Neutrino mass hierarchy.

In a cosmological context, many different parameterizations of the mass hierarchy have been proposed [58–61]. We adopt $r_\nu\equiv(m_3-m_1)/\Sigma m_\nu$ [61] as an additional parameter to nicely discriminate the true neutrino-mass hierarchy pattern from the other between the normal and inverted hierarchies. The normal and inverted mass hierarchies mean $m_1<m_2\ll m_3$ and $m_3\ll m_1<m_2$, respectively. We add r_ν to the fiducial set of the parameters. r_ν becomes positive (negative) for the normal (inverted) hierarchy. It should be a remarkably nice point that the difference between r_ν's of these two hierarchies becomes larger as the total mass Σm_ν becomes smaller. Therefore r_ν is particularly useful for distinguishing the mass hierarchy. In Fig. 2 we plot behaviors of r_ν as a function of Σm_ν. Note that there is a lowest value of Σm_ν which depends on a type of the hierarchies by the neutrino oscillation experiments, i.e., ~ 0.1 eV for the inverted hierarchy and ~ 0.05 eV for the normal hierarchy. Therefore, if we could obtain a clear constraint like $0.05\ {\rm eV}\leqslant\Sigma m_\nu\ll 0.10$ eV, the hierarchy

Table 2
Experimental specifications of Planck, POLARBEAR and CMBPol assumed in this study. Here ν is the observation frequency, Δ_{TT} is the temperature sensitivity per $1' \times 1'$ pixel, Δ_{PP} is the polarization sensitivity per $1' \times 1'$ pixel, θ_{FWHM} is the angular resolution defined as the full width at half-maximum, and f_{sky} is the observed fraction of the sky. We use $\ell_{max} = 2000$ for POLARBEAR, and $\ell_{max} = 2500$ for Planck and CMBPol.

Experiment	ν [GHz]	Δ_{TT} [μK−′]	Δ_{PP} [μK−′]	θ_{FWHM} [′]	f_{sky}
Planck [32]	70	137	195	14	0.65
	100	64.6	104	9.5	0.65
	143	42.6	80.9	7.1	0.65
POLARBEAR [64]	150	–	8	3.5	0.017
CMBPol (EPIC-2m) [65]	70	2.96	4.19	11	0.65
	100	2.29	3.24	8	0.65
	150	2.21	3.13	5	0.65

should be obviously normal without any ambiguities. As will be shown later, however, we can discriminate the hierarchy even when $0.10\ \text{eV} \lesssim \Sigma m_\nu$.

3. CMB

3.1. CMB and neutrino

CMB power spectra are sensitive to neutrino masses. There are three effects that provide detectable signals for the neutrino masses: (1) the transition from relativistic neutrino to nonrelativistic one, (2) smoothing of the matter perturbation by its free-streaming in small scales, and (3) variation of lensed CMB power spectra. Future CMB experiments are expected to set stringent constraints on the sum of neutrino masses [49,62]. In particular, the last effect is unique in the CMB B-mode polarization produced by a CMB lensing. Here we propose to combine the CMB experiments with the 21 cm line observations. As we will see in Section 4, the combined approach resolves degeneracy among some key cosmological parameters and is more powerful than individual CMB measurements. In addition, it is notable that we are able to detect the effective number of neutrino species [63] and determine the neutrino mass hierarchy.

3.2. Sensitivity and analysis of the CMB experiments

In this study, we choose Planck [32], POLARBEAR [64] and CMBPol [65] as examples of CMB experiments. Experimental specifications we assumed are summarized in Table 2.

In our analysis for the CMB, we also take the same fiducial model $(\Omega_m h^2, \Omega h^2, \Omega_\Lambda, n_s, A_s, \tau, Y_{He})$ as that of the 21 cm line experiments (see previous section). We evaluate errors of cosmological parameters by using Fisher matrix, which is given by [56]

$$\mathbf{F}^{CMB}_{ij} = \sum_l \frac{(2\ell+1)}{2} f_{sky} \times \text{Trace}\left[\mathbf{C}_\ell^{-1}\frac{\partial \mathbf{C}_\ell}{\partial p_i}\mathbf{C}_\ell^{-1}\frac{\partial \mathbf{C}_\ell}{\partial p_j}\right]. \tag{8}$$

Here $\mathbf{C}_\ell$ is a covariance matrix constructed by using CMB power spectra C_ℓ^X (X = TT, EE, TE), deflection angle spectrum C_ℓ^{dd}, cross correlation between temperature and deflection angle C_ℓ^{Td}, and noise power spectra N_ℓ^X and N_ℓ^{dd}, where C_ℓ^{dd} is calculated by a lensing potential [68] and is related with C_ℓ^{BB}.[1] We compute N_ℓ^{dd} by using a public code FUTURCMB [69] which adopts the quadratic estimator [68]. In this algorithm, N_ℓ^{dd} is reconstructed by N_ℓ^Y (Y = TT, EE, BB). The covariance matrix in the Fisher matrix is expressed as

$$\mathbf{C}_\ell = \begin{pmatrix} C_\ell^{TT} + N_\ell^{TT} & C_\ell^{TE} & C_\ell^{Td} \\ C_\ell^{TE} & C_\ell^{EE} + N_\ell^{EE} & 0 \\ C_\ell^{Td} & 0 & C_\ell^{dd} + N_\ell^{dd} \end{pmatrix}, \tag{9}$$

where N_ℓ^Y is expressed by using both a beam size $\sigma_{beam}(\nu) = \theta_{FWHM}(\nu)/\sqrt{8\ln 2}$ and an instrumental sensitivity $\Delta_Y(\nu)$ to be

$$N_\ell^Y = \left[\sum_\nu \frac{1}{N_\ell^Y(\nu)}\right]^{-1}, \tag{10}$$

where

$$N_\ell^Y(\nu) = \Delta_Y^2(\nu)\exp\left[\ell(\ell+1)\sigma_{beam}^2(\nu)\right]. \tag{11}$$

For $\Delta_{EE}(\nu)$ and $\Delta_{BB}(\nu)$, we commonly use $\Delta_{PP}(\nu)$ listed in Table 2. N_ℓ^{dd} is calculated by N_ℓ^{TT}, N_ℓ^{EE}, and N_ℓ^{BB}.

In case of Planck and POLARBEAR, we combine both the experiments, and assume that the 1.7% region of the whole sky is observed by both the experiments, and the remaining 63.3% (= 65%–1.7%) region is observed by Planck only. Therefore we evaluate a total Fisher matrix $\mathbf{F}^{CMB}$ by summing the two Fisher matrices,

$$\mathbf{F}^{CMB} = \mathbf{F}^{Planck}(f_{sky} = 0.633) + \mathbf{F}^{Planck+PB}(f_{sky} = 0.017), \tag{12}$$

where $\mathbf{F}^{Planck}$ is the Fisher matrix of the region observed by Planck only and $\mathbf{F}^{Planck+PB}$ is that by both Planck and POLARBEAR.

In addition, we calculate noise power spectra $N_\ell^{Y,Planck+PB}$ of the CMB polarization (Y = EE or BB) in $F^{Planck+PB}$ with the following operation.

(1) $2 \leqslant \ell < 25$, $2000 < \ell \leqslant 2500$

$$N_\ell^{Y,Planck+PB} = N_\ell^{Y,Planck}. \tag{13}$$

(2) $25 \leqslant \ell \leqslant 2000$

$$N_\ell^{Y,Planck+PB} = \left[1/N_\ell^{Y,Planck} + 1/N_\ell^{Y,PB}\right]^{-1}. \tag{14}$$

Since POLARBEAR observes only CMB polarizations, the temperature noise power spectrum $N_\ell^{TT,Planck+PB}$ is equal to $N_\ell^{TT,Planck}$.

In order to combine the CMB experiments with the 21 cm line experiments, we calculate the combined fisher matrix to be

$$\mathbf{F}^{21\,cm+CMB} \simeq \mathbf{F}^{CMB} + \mathbf{F}^{21\,cm}. \tag{15}$$

Here we did not use information for a possible correlation between fluctuations of the 21 cm and the CMB.

4. Results

In this section, we numerically evaluate how we can determine (A) the effective number of neutrino species, and (B) the neutrino mass hierarchy, by combining the 21 cm line observations (MWA, SKA, or Omniscope) with the CMB experiments (Planck + POLARBEAR, or CMBPol). To obtain Fisher matrices we use CAMB [66,67] for calculations of CMB anisotropies C_l and matter power spectra $P_{\delta\delta}$.

[1] By performing a public code HALOFIT [66,67], we have checked that modifications by including nonlinear effects for evolutions of the matter power spectrum are much smaller than typical errors in our analyses and negligible for parameter fittings.

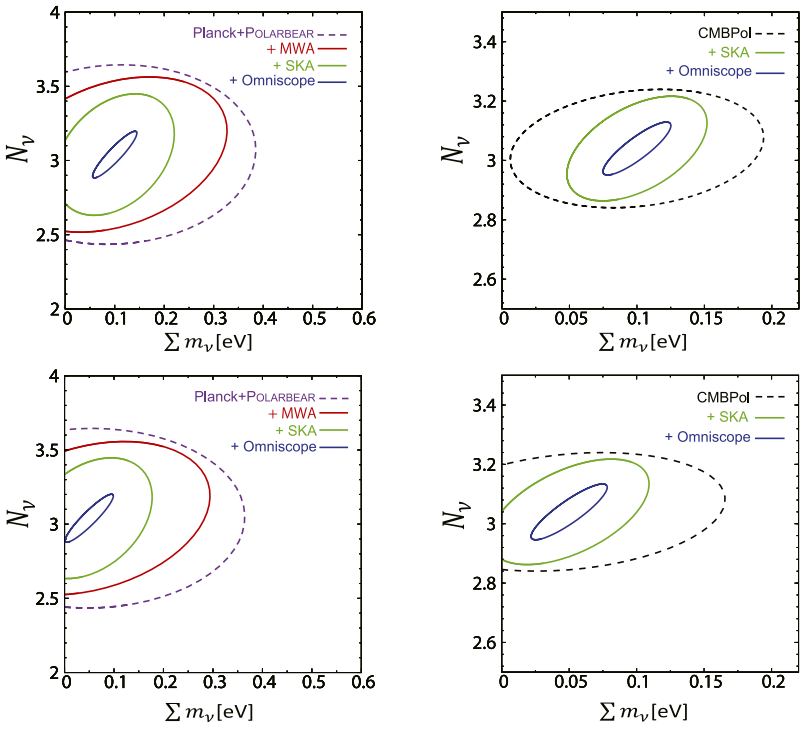

Fig. 1. Contours of 90% C.L. forecasts in Σm_ν–N_ν plane, by adopting Planck + POLARBEAR + each 21 cm experiment (left two panels), or CMBPol + each 21 cm experiment (right two panels). Fiducial values of neutrino parameters, N_ν and Σm_ν, are taken to be $N_\nu = 3.04$ and $\Sigma m_\nu = 0.1$ eV (for upper two panels) or $\Sigma m_\nu = 0.05$ eV (for lower two panels). The dashed line means the constraint obtained by only a CMB observation such as Planck + POLARBEAR alone (left two panels), or CMBPol alone (right two panels). The severer constrains are obtained by combining the CMB with a 21 cm observation such as MWA (outer solid, only for left panels), SKA (middle solid), and Omniscope (inner solid), respectively.

Table 3
1-σ experimental uncertainties of Σm_ν and N_ν, defined by $\Delta p_i = \sqrt{(\mathbf{F}^{-1})_{ii}}$.

Fiducial value	Σm_ν [eV]	N_ν
	0.05	3.04
Planck + POLARBEAR	0.146	0.282
+ MWA	0.114	0.240
+ SKA	0.0592	0.189
+ Omniscope	0.0226	0.0753
CMBPol	0.0538	0.0929
+ SKA	0.0276	0.0827
+ Omniscope	0.0131	0.0438

4.1. Constraints on N_ν

In Fig. 1, we plot contours of 90% confidence levels (C.L.) forecasts in Σm_ν–N_ν plane. The fiducial values of neutrino parameters, N_ν and Σm_ν, are taken to be $N_\nu = 3.04$ and $\Sigma m_\nu = 0.1$ eV (upper two panels), which corresponds to the lowest value of the inverted hierarchy model, or $\Sigma m_\nu = 0.05$ eV (lower two panels), which corresponds to the lowest value of the normal hierarchy model. Adding the 21 cm experiments to the CMB experiment, we see that there is a substantial improvement for the sensitivities to Σm_ν and N_ν. That is because several parameter degeneracies are broken by those combinations, e.g., in particular T_b and As were completely degenerate only in 21 cm line measurements. Therefore it is essential to add the CMB to the 21 cm experiment to be vital for breaking those parameter degeneracies.

If each CMB experiment is combined with SKA or Omniscope, the corresponding constraint can be significantly improved. We showed numerical values of those errors in Table 3 in case that the fiducial values are taken to be $N_\nu = 3.04$ and $\Sigma m_\nu = 0.05$ eV. On the other hand, comparing those values with the current best bounds for $\Sigma m_\nu + N_\nu$ model, which give $\Sigma m_\nu < 0.89$ eV and $N_\nu = 4.47^{+1.82}_{-1.74}$ obtained by CMB (WMAP) + HST (Hubble Space Telescope) + BAO [28], we find that the ongoing and future 21 cm line + the CMB observation will be able to constrain those parameters much more severely.

The case of $\Sigma m_\nu = 0.1$ eV to be fiducial (upper two panels) corresponds to the lowest value for the inverted hierarchy when we use oscillation data. Then it is notable that CMBPol + SKA can detect the nonzero neutrino mass. Of course, Planck + POLARBEAR + Omniscope and CMBPol + Omniscope can obviously do the same job.

On the other hand, the case of $\Sigma m_\nu = 0.05$ eV to be fiducial (lower two panels), which corresponds to the lowest value for the normal hierarchy, only Planck + POLARBEAR + Omniscope or CMBPol + Omniscope can detect the nonzero neutrino mass.

4.2. Constraints on neutrino mass hierarchy

Next we discuss if we will be able to determine the neutrino mass hierarchies by using those ongoing and future 21 cm and CMB observations. In Fig. 2 we plot 2σ errors of the parameter $r_\nu \equiv (m_3 - m_1)/\Sigma m_\nu$ constrained by both the 21 cm and the CMB observations in case of the inverted hierarchy to be fiducial (left), and the normal hierarchy to be fiducial (right). It is notable that the difference between r_ν's of these two hierarchies becomes larger as the total mass Σm_ν becomes smaller. Therefore, r_ν is quite useful to distinguish a true mass hierarchy from the other. Allowed parameters on r_ν by neutrino oscillation experiments are plotted as two bands for the inverted and the normal hierarchies, respectively. The thin solid lines inside the bands are the experimental mean values by oscillations, one of which is taken to be a corresponding fiducial value of r_ν as a function of Σm_ν in each analysis. The constrains are obtained by combining Omniscope with Planck + POLARBEAR (thick

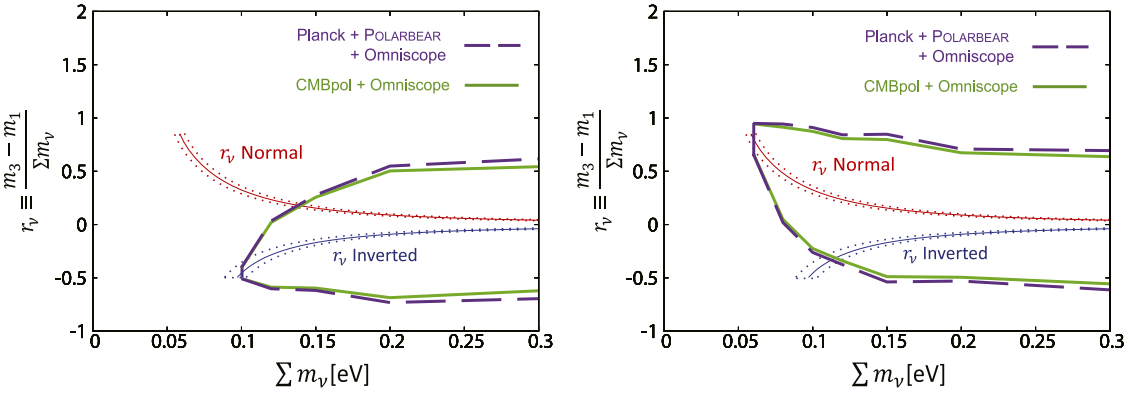

Fig. 2. Forecasts of 2σ errors on $r_\nu = (m_3 - m_1)/\Sigma m_\nu$ constrained by both the 21 cm and the CMB observations in case of the inverted hierarchy to be fiducial (left), and the normal hierarchy to be fiducial (right). The constrains are obtained by combining Omniscope with Planck + POLARBEAR (thick dashed lines), and Omniscope with CMBPol (thick solid lines), respectively. Allowed parameters on r_ν by neutrino oscillation experiments are plotted as two bands for the inverted and the normal hierarchies, respectively (the name of each hierarchy is written in the close vicinity of the line). The solid line inside the band is the fiducial value of r_ν as a function of Σm_ν.

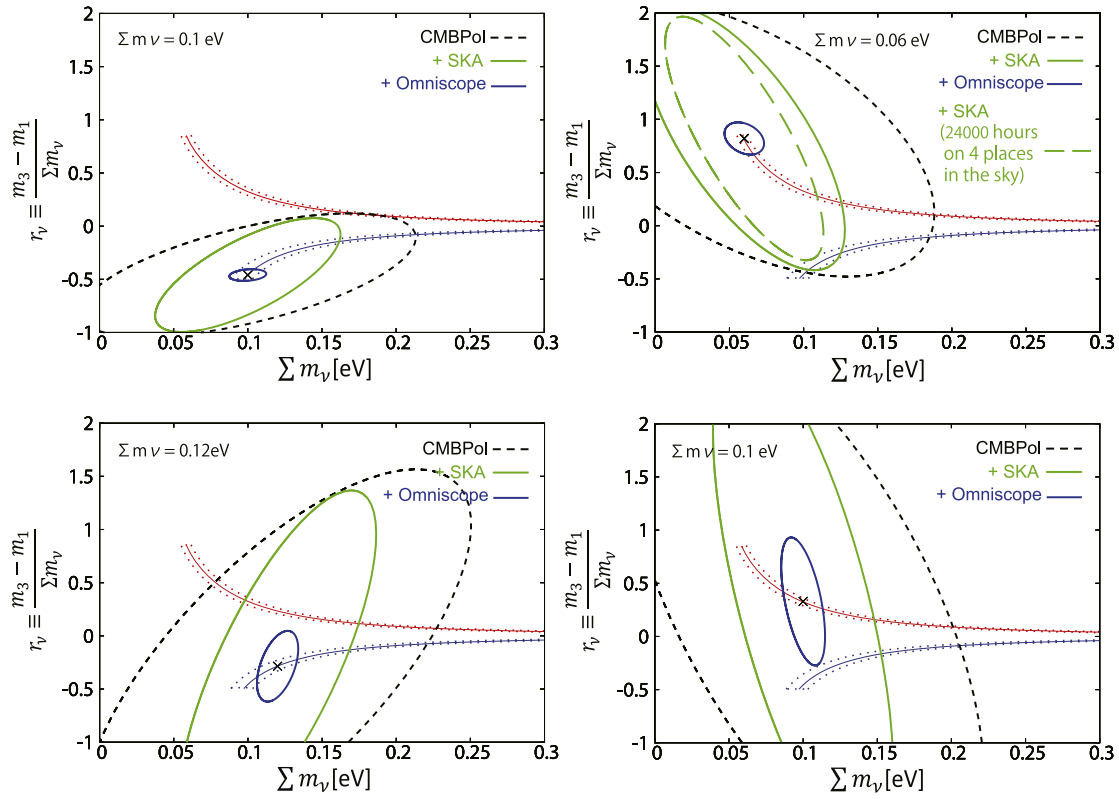

Fig. 3. Contours of 90% C.L. forecasts in Σm_ν–r_ν plane, by adopting CMBPol + each 21 cm experiment. Fiducial value of Σm_ν and the mass hierarchy (diagonal cross) are taken to be: $\Sigma m_\nu = 0.1$ eV and the inverted (for left upper panel), $\Sigma m_\nu = 0.12$ eV and the inverted (for left lower panel), $\Sigma m_\nu = 0.06$ eV and the normal (for right upper panel), $\Sigma m_\nu = 0.1$ eV and the normal (for right lower panel). The short dashed lines mean the constraints obtained by only a CMBPol observation, and the long dashed line means the one by a SKA + CMBPol observation for 24 000 h on four places in the sky. The outer (inner) solid line means combining the CMBPol with SKA (Omniscope). Allowed parameters on r_ν by neutrino oscillation experiments are plotted in the same way of Fig. 2.

dashed lines) and Omniscope with CMBPol (thick solid lines), respectively.

For 0.3 eV $\lesssim \Sigma m_\nu$ the mass eigenvalues m_1, m_2, and m_3 are almost degenerate. Therefore the difference between two hierarchies has little influence on the matter power spectrum. Therefore the constraints on r_ν are significantly weak compared with the difference between them, and then we cannot distinguish the true hierarchy from the other.

On the other hand however, the difference increases as Σm_ν decreases down to $m_\nu \sim 0.1$ eV. By using this property, the CMB (Planck + POLARBEAR or CMBPol) + the 21 cm (Omniscope) observations can constrain the neutrino mass hierarchy severely. Typically errors of Σm_ν at around $\Sigma m_\nu = 0.1$ eV are given by $\Delta\Sigma m_\nu = 0.0087$ eV for Planck + POLARBEAR, and $\Delta\Sigma m_\nu = 0.0069$ eV for CMBPol at 1σ, respectively. Therefore, the error of the x-axis is negligible compared with that of y-axis. In Fig. 3, we plot contours of 90% C.L. in Σm_ν–r_ν plane in order to show errors of Σm_ν along the x-axis for typical fiducial values. As is clearly shown in Fig. 2, actually those combinations of the observations will be able to determine the neutrino mass hierarchy to be inverted or normal for $\Sigma m_\nu \lesssim 0.13$ eV or $\Sigma m_\nu \lesssim 0.1$ eV at 90% C.L., respectively. Although the determination is possible only at around $\Sigma m_\nu \lesssim \mathcal{O}(0.1)$ eV, those results should be reasonable. That is because a precise discrimination of the mass hierarchy itself

may have no meaning if the masses are highly degenerate, i.e., if $\Sigma m_\nu \gg 0.1$–0.3 eV.

Once a clear signature $\Sigma m_\nu \ll 0.1$ eV were determined by observations or experiments, it should be obvious that the hierarchy must be normal without any ambiguities. On the other hand if the hierarchy were inverted, we could not determine it only by using Σm_ν. However, it is remarkable that our method is quite useful because we can discriminate the hierarchy from the other even if the fiducial values were $\Sigma m_\nu \gtrsim 0.1$ eV for both the normal and inverted cases. This is clearly shown in Fig. 3. In case that a fiducial value of Σm_ν is taken to be the lowest values in neutrino oscillation experiments, the upper left (right) figure indicates that even CMBPol + SKA can discriminate the inverted (normal) mass hierarchy from the normal (inverted) one.

5. Conclusions

We have studied how we can constrain effective number of neutrino species N_ν, total neutrino masses Σm_ν, and neutrino mass hierarchy by using the 21 cm observations (MWA, SKA, and Omniscope) and the CMB observations (Planck, POLARBEAR, and CMBPol). It is essential to combine the 21 cm with the CMB B-mode polarization produced by a CMB lensing to break various degeneracies in cosmological parameters when we perform multiple-parameter fittings.

About the constraints on Σm_ν–N_ν plane, for a fiducial value $\Sigma m_\nu = 0.1$ eV which corresponds to the lowest value in the inverted hierarchy, we have found that CMBPol + SKA, Planck + POLARBEAR + Omniscope and CMBPol + Omniscope can detect the nonzero neutrino mass. For a fiducial value $\Sigma m_\nu = 0.05$ eV, which corresponds to the lowest value in the normal hierarchy, Planck + POLARBEAR + Omniscope or CMBPol + Omniscope can detect the nonzero neutrino mass.

As for the determination of the neutrino mass hierarchy, we have proposed a new parameter $r_\nu = (m_3 - m_1)/\Sigma m_\nu$ and studied how to discriminate a true hierarchy from the other by constraining r_ν. As was clearly shown in Fig. 2, the combinations of the CMB (Planck + POLARBEAR or CMBPol) + the 21 cm (Omniscope) will be able to determine the hierarchy to be inverted or normal for $\Sigma m_\nu \lesssim 0.13$ eV or $\lesssim 0.1$ eV at 2σ, respectively. Furthermore, if the fiducial value of Σm_ν is taken to be the lowest value in the neutrino oscillation experiments, even CMBPol + SKA can determine the mass hierarchy.

In this study we have taken the simplified model of reionization. In case of more likely detailed modeling of reionization [45], it was pointed out that the constraints on cosmological parameters may moderately change at $\sim$ 10–50%. Fortunately, this effect is comparatively small and should not be fatal to constrain the neutrino mass hierarchy in the current analyses.

Acknowledgements

We thank M. Hazumi, K. Ioka, H. Kodama, R. Nagata, T. Namikawa, M. Takada and A. Taruya for useful discussions. This work is supported in part by Grant-in-Aid for Scientific research from the Ministry of Education, Science, Sports, and Culture (MEXT), Japan, No. 245516 (A.S.), Nos. 21111006, 22244030, and 23540327 (K.K.).

References

[1] B. Aharmim, et al., SNO Collaboration, Phys. Rev. Lett. 101 (2008) 111301.
[2] P. Adamson, et al., MINOS Collaboration, Phys. Rev. Lett. 101 (2008) 131802, arXiv:0806.2237 [hep-ex].
[3] T. Thummler, KATRIN Collaboration, Phys. Part. Nucl. 42 (2011) 590; M. Beck, KATRIN Collaboration, J. Phys. Conf. Ser. 203 (2010) 012097, arXiv:0910.4862 [nucl-ex].
[4] J.J. Gomez-Cadenas, J. Martin-Albo, M. Sorel, P. Ferrario, F. Monrabal, J. Munoz-Vidal, P. Novella, A. Poves, JCAP 1106 (2011) 007, arXiv:1010.5112 [hep-ex].
[5] INO, India Based Neutrino Observatory, URL http://www.ino.tifr.res.in/ino/.
[6] M. Blennow, T. Schwetz, arXiv:1203.3388 [hep-ph].
[7] E.K. Akhmedov, S. Razzaque, A.Y. Smirnov, arXiv:1205.7071 [hep-ph].
[8] D.S. Ayres, et al., NOvA Collaboration, hep-ex/0503053.
[9] M. Ishitsuka, T. Kajita, H. Minakata, H. Nunokawa, Phys. Rev. D 72 (2005) 033003, hep-ph/0504026.
[10] K. Hagiwara, N. Okamura, K.-i. Senda, Phys. Lett. B 637 (2006) 266; K. Hagiwara, N. Okamura, K.-i. Senda, Phys. Lett. B 641 (2006) 491 (Erratum), hep-ph/0504061.
[11] A. Badertscher, T. Hasegawa, T. Kobayashi, A. Marchionni, A. Meregaglia, T. Maruyama, K. Nishikawa, A. Rubbia, arXiv:0804.2111 [hep-ph].
[12] S.K. Agarwalla, P. Hernandez, arXiv:1204.4217 [hep-ph].
[13] O. Elgaroy, O. Lahav, JCAP 0304 (2003) 004, astro-ph/0303089.
[14] K. Ichikawa, M. Fukugita, M. Kawasaki, Phys. Rev. D 71 (2005) 043001.
[15] U. Seljak, et al., SDSS Collaboration, Phys. Rev. D 71 (2005) 103515, astro-ph/0407372.
[16] A. Goobar, S. Hannestad, E. Mortsell, H. Tu, JCAP 0606 (2006) 019, astro-ph/0602155.
[17] K. Ichiki, M. Takada, T. Takahashi, Phys. Rev. D 79 (2009) 023520.
[18] S.A. Thomas, F.B. Abdalla, O. Lahav, Phys. Rev. Lett. 105 (2010) 031301, arXiv:0911.5291 [astro-ph.CO].
[19] S. Riemer-Sorensen, C. Blake, D. Parkinson, T.M. Davis, S. Brough, M. Colless, C. Contreras, W. Couch, et al., Phys. Rev. D 85 (2012) 081101, arXiv:1112.4940 [astro-ph.CO].
[20] S. Hannestad, A. Mirizzi, G.G. Raffelt, Y.Y.Y. Wong, JCAP 1008 (2010) 001.
[21] S. Saito, M. Takada, A. Taruya, Phys. Rev. D 83 (2011) 043529.
[22] P. Crotty, J. Lesgourgues, S. Pastor, Phys. Rev. D 69 (2004) 123007, hep-ph/0402049.
[23] U. Seljak, A. Slosar, P. McDonald, JCAP 0610 (2006) 014, astro-ph/0604335.
[24] M. Fukugita, K. Ichikawa, M. Kawasaki, O. Lahav, Phys. Rev. D 74 (2006) 027302.
[25] E. Komatsu, et al., WMAP Collaboration, Astrophys. J. Suppl. 180 (2009) 330, arXiv:0803.0547 [astro-ph].
[26] B.A. Reid, W.J. Percival, D.J. Eisenstein, L. Verde, D.N. Spergel, R.A. Skibba, N.A. Bahcall, T. Budavari, et al., Mon. Not. Roy. Astron. Soc. 404 (2010) 60, arXiv:0907.1659 [astro-ph.CO].
[27] B.A. Reid, L. Verde, R. Jimenez, O. Mena, JCAP 1001 (2010) 003, arXiv:0910.0008 [astro-ph.CO].
[28] J. Hamann, S. Hannestad, J. Lesgourgues, C. Rampf, Y.Y.Y. Wong, JCAP 1007 (2010) 022, arXiv:1003.3999 [astro-ph.CO].
[29] E. Komatsu, et al., WMAP Collaboration, Astrophys. J. Suppl. 192 (2011) 18, arXiv:1001.4538 [astro-ph.CO].
[30] E. Pierpaoli, Mon. Not. Roy. Astron. Soc. 342 (2003) L63, astro-ph/0302465.
[31] P. Crotty, J. Lesgourgues, S. Pastor, Phys. Rev. D 67 (2003) 123005, astro-ph/0302337.
[32] J. Lesgourgues, L. Perotto, S. Pastor, M. Piat, Phys. Rev. D 73 (2006) 045021, astro-ph/0511735.
[33] R. de Putter, O. Zahn, E.V. Linder, Phys. Rev. D 79 (2009) 065033.
[34] S. Furlanetto, S.P. Oh, F. Briggs, Phys. Rept. 433 (2006) 181.
[35] A. Loeb, S. Wyithe, Phys. Rev. Lett. 100 (2008) 161301.
[36] J.R. Pritchard, E. Pierpaoli, Phys. Rev. D 78 (2008) 065009.
[37] K.N. Abazajian, E. Calabrese, A. Cooray, F. De Bernardis, S. Dodelson, A. Friedland, G.M. Fuller, S. Hannestad, et al., Astropart. Phys. 35 (2011) 177, arXiv:1103.5083 [astro-ph.CO].
[38] J.R. Pritchard, A. Loeb, arXiv:1109.6012 [astro-ph.CO].
[39] P. Madau, A. Meiksin, M.J. Rees, Astrophys. J. 475 (1997) 429, arXiv:astro-ph/9608010.
[40] S. Furlanetto, Mon. Not. Roy. Astron. Soc. 371 (2006) 867, arXiv:astro-ph/0604040.
[41] J.R. Pritchard, A. Loeb, Phys. Rev. D 78 (2008) 103511, arXiv:0802.2102 [astro-ph].
[42] S.A. Wouthuysen, Astron. J. 57 (1952) 31.
[43] G.B. Field, Proc. IRE 46 (1958) 240.
[44] J.R. Pritchard, E. Pierpaoli, Nucl. Phys. Proc. Suppl. 188 (2009) 31.
[45] Y. Mao, M. Tegmark, M. McQuinn, M. Zaldarriaga, O. Zahn, Phys. Rev. D 78 (2008) 023529, arXiv:0802.1710 [astro-ph].
[46] S. Joudaki, O. Dore, L. Ferramacho, M. Kaplinghat, M.G. Santos, Phys. Rev. Lett. 107 (2011) 131304, arXiv:1105.1773 [astro-ph.CO].
[47] E. Chapman, F.B. Abdalla, G. Harker, V. Jelic, P. Labropoulos, S. Zaroubi, M.A. Brentjens, A.G. de Bruyn, et al., arXiv:1201.2190 [astro-ph.CO].
[48] http://www.lofar.org/.
[49] J. Lesgourgues, S. Pastor, Phys. Rept. 429 (2006) 307, arXiv:astro-ph/0603494.
[50] J. Lesgourgues, S. Pastor, L. Perotto, Phys. Rev. D 70 (2004) 045016, hep-ph/0403296.
[51] http://www.mwatelescope.org/.

[52] http://www.skatelescope.org/.
[53] M. Tegmark, M. Zaldarriaga, Phys. Rev. D 82 (2010) 103501, arXiv:0909.0001 [astro-ph.CO].
[54] S. Wyithe, M.F. Morales, arXiv:astro-ph/0703070.
[55] J.D. Bowman, M.F. Morales, J.N. Hewitt, Astrophys. J. 638 (2006) 20, arXiv:astro-ph/0507357.
[56] M. Tegmark, A. Taylor, A. Heavens, Astrophys. J. 480 (1997) 22, arXiv:astro-ph/9603021.
[57] M. McQuinn, O. Zahn, M. Zaldarriaga, L. Hernquist, S.R. Furlanetto, Astrophys. J. 653 (2006) 815, arXiv:astro-ph/0512263.
[58] M. Takada, E. Komatsu, T. Futamase, Phys. Rev. D 73 (2006) 083520, astro-ph/0512374.
[59] A. Slosar, Phys. Rev. D 73 (2006) 123501, astro-ph/0602133.
[60] F. De Bernardis, T.D. Kitching, A. Heavens, A. Melchiorri, Phys. Rev. D 80 (2009) 123509, arXiv:0907.1917 [astro-ph.CO].
[61] R. Jimenez, T. Kitching, C. Pena-Garay, L. Verde, JCAP 1005 (2010) 035, arXiv:1003.5918 [astro-ph.CO].
[62] Y.Y.Y. Wong, Ann. Rev. Nucl. Part. Sci. 61 (2011) 69, arXiv:1111.1436 [astro-ph.CO].
[63] Z. Chacko, L.J. Hall, T. Okui, S.J. Oliver, Phys. Rev. D 70 (2004) 085008, hep-ph/0312267.
[64] H. Nishino, et al., in: Proceedings of the 47th Rencontres de Moriond Cosmology, 2012.
[65] D. Baumann, et al., CMBPol Study Team Collaboration, AIP Conf. Proc. 1141 (2009) 10, arXiv:0811.3919 [astro-ph].
[66] A. Lewis, A. Challinor, A. Lasenby, Astrophys. J. 538 (2000) 473, astro-ph/9911177.
[67] http://camb.info/.
[68] T. Okamoto, W. Hu, Phys. Rev. D 67 (2003) 083002, astro-ph/0301031.
[69] http://lpsc.in2p3.fr/perotto/.